AIAA JOURNAL
Vol. 40, No. 9, September 2002

Midfrequency Vibrations of a Complex Structure: Experiments and Comparison with Numerical Simulations

Eric Savin*
ONERA, 92322 Châtillon, France

The results of an experimental study of the vibrations of a complex, three-dimensional heterogeneous structure under broadband excitations and comparisons with numerical simulations are presented. The so-called midfrequency range is exhibited for the tested structure, and a modeling strategy is proposed on the basis of physical observations from the measured frequency response functions and mechanical energies. A time-frequency algorithm is used for the numerical analyses at the intermediate frequencies, which reveal the current shortcomings of the available numerical methods.

Nomenclature

$\mathcal{B}$	=	overall frequency band
B_ν	=	νth narrow midfrequency band
$\boldsymbol{D}$	=	structural damping matrix
$\langle E_{s,\nu}\rangle$	=	estimated mechanical energy in the sth segment and νth narrow frequency band
$\langle e_s(\omega)\rangle$	=	estimated mechanical energy density in the sth segment
$\boldsymbol{F}_\nu$	=	vector of nodal forces in the νth narrow frequency band
i	=	$\sqrt{-1}$
$\boldsymbol{K}$	=	structural stiffness matrix
$\boldsymbol{M}$	=	structural mass matrix
m_j	=	mass of the jth plate
N	=	number of degrees of freedom
N_{plate}	=	number of plates in a structural segment
q_α	=	αth generalized coordinate
t	=	time
$\boldsymbol{U}_\nu$	=	vector of nodal displacements in the νth narrow frequency band
$\underset{\sim}{U}_\nu$	=	approximated vector of nodal displacements in the νth narrow frequency band
$\boldsymbol{V}$	=	perturbation of the structural stiffness matrix
$V_{\alpha\beta}$	=	$\alpha\beta$th element of $\boldsymbol{V}$
v_{jk}	=	measured normal velocity by the kth accelerometer of the jth plate
$\Delta\omega_\nu$	=	bandwidth of the νth narrow midfrequency band
δ_{jk}	=	Kronecker symbol: $\delta_{jk}=1$ if $j=k$, $\delta_{jk}=0$ if $j\neq k$
ζ_ν	=	average structural damping rate in the νth narrow midfrequency band
τ	=	generic stiffness parameter
$\boldsymbol{\phi}_\alpha$	=	αth structural eigenmode
$\tilde{\boldsymbol{\phi}}_\alpha$	=	αth eigenmode of the perturbed structure
Ω_ν	=	central frequency of the νth narrow midfrequency band
ω	=	circular frequency
ω_α	=	αth structural eigenfrequency
$\tilde{\omega}_\alpha$	=	αth eigenfrequency of the perturbed structure
$\mathbf{1}_I$	=	indicator function of a set I

Received 17 October 2001; revision received 26 March 2002; accepted for publication 16 April 2002.

*Research Engineer, Structural Dynamics and Coupled Systems Department, B.P. 72, 29 Avenue de la Division Leclerc; Eric.Savin@onera.fr.

Introduction

LOW-FREQUENCY linear vibrations of complex, industrial structures can be predicted efficiently by reduced numerical models of limited size. They are constructed by a Ritz–Galerkin projection on a finite number of eigenmodes associated to the first eigenvalues of the conservative structure. Their efficiency is because only a low number of generalized degrees of freedom are used in this type of representation. These models, eventually updated by appropriate methods,[1] usually compare very well with experimental data at low frequencies but can deteriorate rapidly when the frequency is increased. That such techniques are less adapted to the higher-frequency ranges originates from numerical, but above all, more fundamental physical reasons. The objective of the present work is threefold. First, we show from extensive experiments some characteristic features of the vibrational behavior of a truly complex structure in the higher-frequency ranges. Second, we deduce a possible modeling strategy from these observations. Third, we compare to our experimental data the numerical results obtained with a particular simulation method adapted to the prediction of vibrations in the so-called midfrequency range, and we discuss the relevance of that method.

A "complex" structure is defined in the frame of the present study as a mechanical system constituted by the assembly of several more simple subsystems, such as beams, plates, cylindrical shells. The latter can also have high stiffness contrasts. Complexity can also be introduced by secondary equipments attached to a main structure, already complex in itself, but this aspect is presently ignored in this communication. Midfrequencies are defined as the intermediate frequencies for which the structure has neither a modal behavior as in the low-frequency range nor a smoothed diffusive-like behavior as in the high-frequency range. A truly complex, three-dimensional structure of large size is tested under broadband excitations in order to describe more precisely, from phenomenological observations, the various frequency domains.

From these experiments we wish to draw a tentative modeling strategy for midfrequency vibrations as they were already defined. Several numerical methods have been proposed in the literature to tackle such a problem. They can be arbitrarily divided into three classes. A first approach consists in extending the usual numerical methods adapted to low-frequency predictions, typically the finite element method, to the midfrequency range. Researchers have considered either higher-order and/or hierarchical finite elements,[2,3] or multiscales finite elements in the space variable,[4–6] time variable[7,8] or both,[9,10] or spectral approaches,[11] or coupled finite elements and integral representations.[12] The second approach consists in extending the analysis methods adapted to high-frequency predictions to the midfrequency range. The influence of global eigenmodes of vibration in statistical energy analysis (SEA)[13,14] or in a power flow approach,[15] for instance, is considered in some hybrid methods. Asymptotic ray methods may also be applied.[16] The third class of methods consists in using some specific reduction bases adapted to

the intermediate frequency range.[17–21] The choice of one of these methodologies for numerical simulations of the complex structure studied here shall be guided by the observations done from experiments.

In the next section we start by briefly presenting the complex structure in question, as well as the experimental setup and the measurements made. Then in a subsequent section we detail the various results obtained and give tentative physical interpretations, highlighting particularily the intermediate frequency range. We also underline the implications of the observed behavior on the modeling strategy to be adopted, especially in view of the assumed linearity of the structure, the trends of its frequency response and mechanical energy distribution, and the influence of uncertainties. In the fourth section we present the results of numerical simulations for the time-frequency algorithm developed in Refs. 7–9, which is found to be a priori well adapted to the problem at hand, and can be rather straightforwardly implemented in any commercial finite element code. We finally draw some conclusions and perspectives on further developments on the basis of the comparisons of these numerical results with the experimental ones and especially the actual limitations of the numerical methods currently implemented.

Description of the Structure and Experimental Setup

We give here only the minimum necessary information on the tested structure and the experimental setup. More details are given in Ref. 22.

Geometry and Mechanical Characteristics of the Structure

The experimental structure is made of aluminum alloy. An overview of its geometry can be seen on the CAD view of Fig. 1. Its cross-section characteristics are summarized in Fig. 2. It is 5.3 m long, 2.5 m wide, and 1.4 m high and comprises about 200 plates, 400 stiffeners, and 54 cavities. It is divided along its longitudinal axis noted y into nine compartments, or segments, seperated by vertical bulkheads constituted by nonstiffened plates. The compartments were assigned different lengths to break the periodicity. All plates have a thickness of 1.2 mm, and their mechanical characteristics are given in Table 1 together with those of the stiffeners and the ribs and stringers, which constitute the main frame. These properties were measured from samples of the various elements used. The experimental structure has been weighted, and its total mass is 825 kg.

The longitudinal elements of the main frame are continuous (welded), its transverse (x axis) and vertical (z axis) ribs and stringers being welded to the longitudinal ones. Rivets are used for all junctions of the plates with the main frame and the ribs and stringers, with an average spacing of 5 cm. The stiffeners are riveted to the plates with an average spacing of 5 cm as well. This length corresponds to wavelengths at 1162 Hz for the present materials. The average spacing between stiffeners is 20 cm (see Fig. 2).

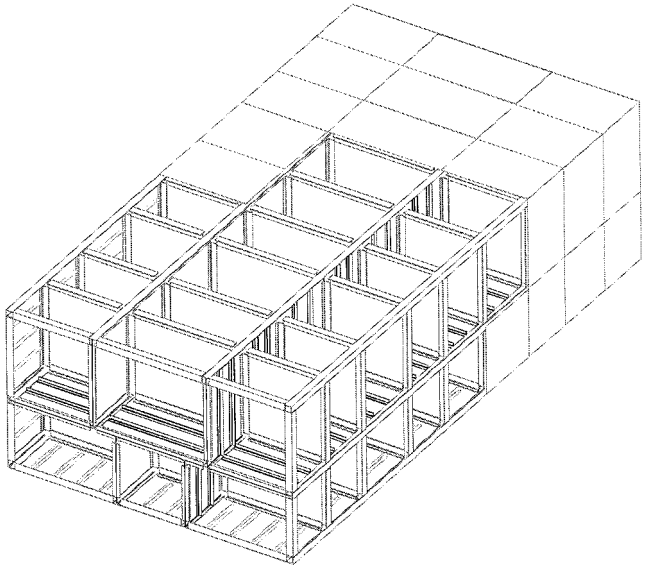

Fig. 1 CAD view of the experimental structure. The structure is entirely closed for experiments, but some outer plates have been removed on the sketch to make its main frame visible.

Table 1 Mechanical characteristics of the structural elements

Structural element	Density, kg/m^3	Young's modulus, N/m^2
Plate	2670	6.30×10^{10}
Stiffener	2700	6.23×10^{10}
Stringer/frame	2700	6.95×10^{10}

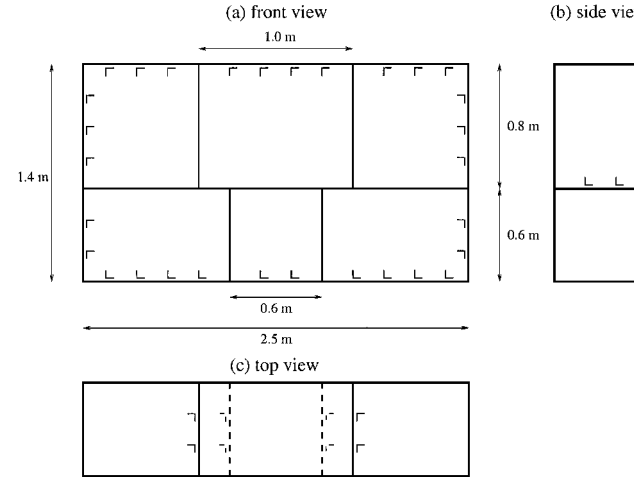

Fig. 2 Sketches of a typical segment with positioning of the L-shaped 30 × 30 × 3 mm stiffeners: a) cross section (front view) with the stiffeners on the outer plates, b) side view with the stiffeners on the intermediate floor, and c) top view with the stiffeners on the inner bulkheads.

Fig. 3 Experimental complex structure in testing configuration.

Experimental Setup

The structure is suspended by means of eight rubber extensible springs, the overall frequency of suspension being 1.84 Hz, which is well below the frequency range of interest. Therefore the structure is considered to have free-free boundary conditions in the analysis. Figure 3 is a photograph of the structure in testing configuration.

To eliminate the contributions of internal acoustics, foams have been suspended in all cavities. It has been shown by additional experiments[22] that a filling rate of 10% of the cavities' volume is sufficient for the erasure of acoustic modes in the midfrequency range of interest, up to about 1200 Hz (see the following).

Four sets of accelerometers are distributed on the structure (see Fig. 4). The first set is positioned along the upper-right-hand corner in the longitudinal direction y in order to capture the global vibration modes of the structure: 10 B&K 4371 triaxial sensors are positioned

right at each bulkhead between two segments and the extremities of the structure. The second set contains 69 miniature accelerometers distributed randomly on the 23 plates constituting the first segment, including the 6 nonstiffened plates of the bulkhead between this segment and the second one. Three accelerometers are provided on each plate. The third and fourth sets are similar in principle to the second one, the accelerometers being distributed randomly as well on the fifth and ninth segments respectively. Three types of low mass sensors are used in these sets: B&K 8307, B&K 4375, and B&K 4374. Their purpose is to estimate the mechanical energies in the equipped segments. Finally accelerometers were installed at each of the four excitation locations (see the following) in order to measure the autotransfers. These accelerometers and the four preceding sets amount to a total number of 240 sensors, for which acquisitions were made in four sequences up to 10,000 Hz.

White-noise excitations are successively applied at four points at one extremity of the structure (see Fig. 4 for their locations and labels). They are generated by an electrodynamic exciter connected to a force gauge developed at ONERA, whose parasitic mass is less than 0.5 g. Examination of input powers and ordinary coherencies indicated that all measurements were fully workable in the frequency range 50–5000 Hz (Ref. 22).

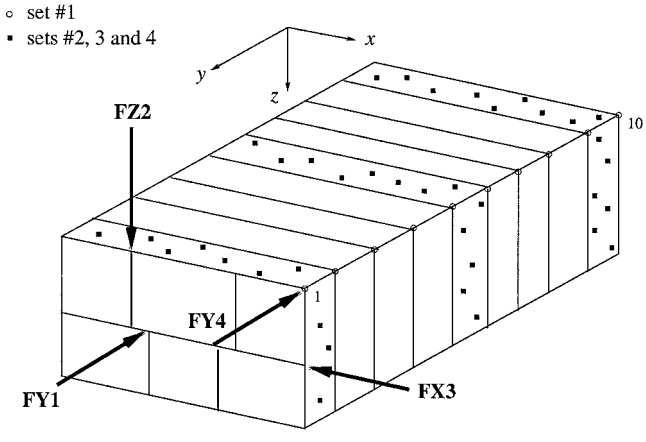

Fig. 4 Locations of the applied excitations and sets of accelerometers. Only several accelerometers of sets 2–4 have been displayed on this sketch, for illustration purposes.

Midfrequency Vibrations of the Experimental Structure: Measurements and Mechanical Interpretation

Linearity of the Structure

Were the structure perfectly linear throughout the whole frequency range considered, reciprocity would be observed at any frequency. Figure 5 compares the frequency response function (acceleration) measured at the location and direction of excitation FY4 when excitation FY1 is applied, and the frequency response function measured at the location and direction of excitation FY1 when excitation FY4 is applied. It is seen that these two curves are almost identical up to about 1200 Hz, which is in agreement with the cutoff frequency estimated from the average spacing between the rivets. Beyond this frequency nonproportional damping and nonlinear effects are introduced locally by the riveted joints of the various structural elements. For an analyis at these frequencies, they can be taken into account through for instance loss factors in an energetic approach, as done in SEA; this of course cannot permit the recovery of the discrepencies observed for the frequency response functions. Up to the cutoff frequency just outlined, it is expected that structural vibrations can be well predicted by the classical theory of linear elasticity, including damping and a proper representation of the boundary conditions.

Illustration of the Midfrequency Range

As a first illustrative example of the various measurements done on the experimental structure described in the preceding section, we plot on Fig. 6 the estimated mechanical energy densities $\langle e(\omega)\rangle$ for segments 1 (at the extremity of the structure where the loads are applied), 5 (intermediate), and 9 (the other extremity) in the frequency range 50–5000 Hz. Mechanical energies in each segment are estimated by

$$\langle e_s(\omega)\rangle = \sum_{j=1}^{N_{\text{plate}}} \frac{m_j}{3} \sum_{k=1}^{3} |v_{jk}(\omega)|^2 \tag{1}$$

where $s = 1$, 5, or 9 for either segment 1, 5, or 9.

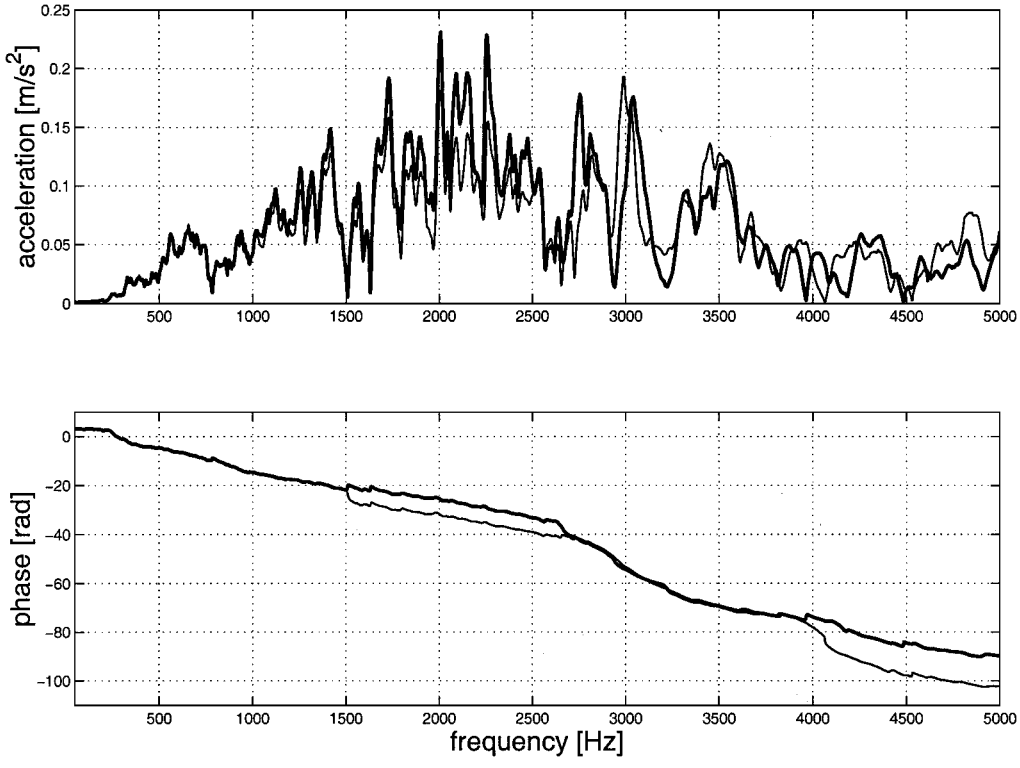

Fig. 5 Comparison of cross transfers for excitations FY1 and FY4.

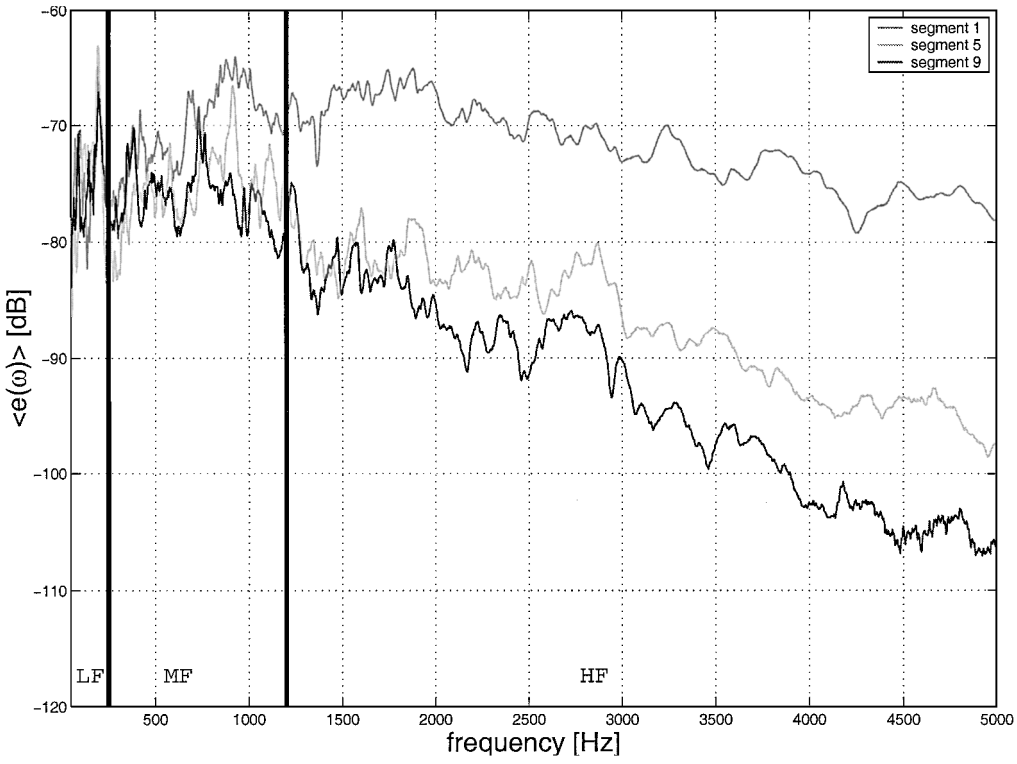

Fig. 6 Estimated mechanical energy densities for segments 1, 5, and 9 and excitation FX3. $dB_{ref} = 10 \times \log_{10}(1\ kg \cdot m^2/s^2)$.

This plot displays three characteristic frequency domains denoted by LF, HF, and MF in Fig. 6. In the low-frequency range (LF), here for frequencies up to about 250 Hz, the estimated mechanical energies have the same levels for the three segments, although they are rapidly varying. Thus for such frequencies the vibratory energy propagates broadly to the entire structure and does not remain localized near the excitation. On the contrary in the high-frequency range (HF), here for frequencies higher than about 1200 Hz, the energy levels decrease significantly when observed at increased distances from the excitation. They are also steadily decreasing with the frequency. Thus for such frequencies the vibratory energy remains localized close to the excitation and diffuses only weakly to the other parts of the structure. For the intermediate frequencies, the so-called midfrequency range (MF), the general trend is that the energy levels in segments 5 and 9 are comparable but lower than the one in segment 1. Thus the vibratory energy gets partially localized close to the excitation, the remaining being spread in the entire structure as is the case in the low-frequency range. In some narrow subbands, however, one can observe that energies in segment 5 or 9 or both are comparable with the energy in segment 1. This is also to be expected from a typical midfrequency dynamic behavior because it is at the transition between the low- and high-frequency ones. It outlines in the mean time the necessity of having an information on the phase in that intermediate frequency range.

Figure 7 displays the vertical accelerations measured by the accelerometers 1, 4, and 9 of the first set: they are located along the upper right corner of the structure in the longitudinal direction y, accelerometer 1 being the closest one to the excitation, accelerometer 4 being at an intermediate position, and accelerometer 9 being located at the other extremity of the structure. The same general remarks as for localization or not of the vibrational energy hold for the acceleration amplitudes shown, with an additional information given here by the phase. In the high-frequency range it is uniformly decreasing and follows the same trend for the three accelerometers. Thus it brings no additional knowledge on the vibrational state of the structure from one point to another. On the other hand, it is strongly varying between $-\pi$ and $+\pi$ (phase jumps correspond to the resonances) in the low-frequency range, for which it constitutes an essential characteristic of the vibrational state of the structure. In the intermediate-frequency range the phase is significantly decreasing; however, it follows different trends from one point to another. Thus it constitutes an important characteristic of the vibrational state in this frequency domain. This means that energy-type quantities are not sufficient to describe midfrequency vibrations as just defined in the context of the present experimental observations: one might be able to provide an information on the phase as well (from measurement or simulation of local quantities). This important point has also been underlined in the recent work of Ref. 15 dedicated to the development of a numerical method for the prediction of the vibrations at these intermediate frequencies.

From a mechanical point of view, the three frequency domains just exhibited are characterized in the following way:

1) Low frequencies correspond to the first vibrational eigenmodes of the entire structure, the modal density (provided that it can be defined in this domain, which is rather unclear) being low.

2) High frequencies correspond to the frequency ranges where the modal density exhibits high, rather uniform values over these ranges. In this case energy-type quantities smoothing the contributions from the various eigenmodes in a given frequency band are more adapted to the characterization of the vibratory state of the structure, especially because the phase does not bring any additional information.

3) Medium frequencies corresponds to the frequency ranges where the modal density exhibits important variations from one band to the other. Vibrations of a complex structure are characterized by the superposition of some global eigenmodes and clusters of local eigenmodes,[23] which have an influence on both the local and global behaviors of the structure in the narrow frequency band where they are packed.

The local modes just introduced do not necessarily have a highly oscillating shape. For instance, vibrations of three-dimensional truss structures typically exhibit such a behavior because of the numerous, densely packed eigenmodes associated to all of the repetitive truss members (beams and frames), which exist even at relatively low frequencies.[20,21] In the present case, modal clusters do occur because of the repetitive (although nonperiodic) nature of the experimental structure. They are associated to the local eigenmodes of the various plates constituting it, which have comparable geometrical and mechanical characteristics. Because of this occurence, uncertainties play a fundamental role as shown in the next section.

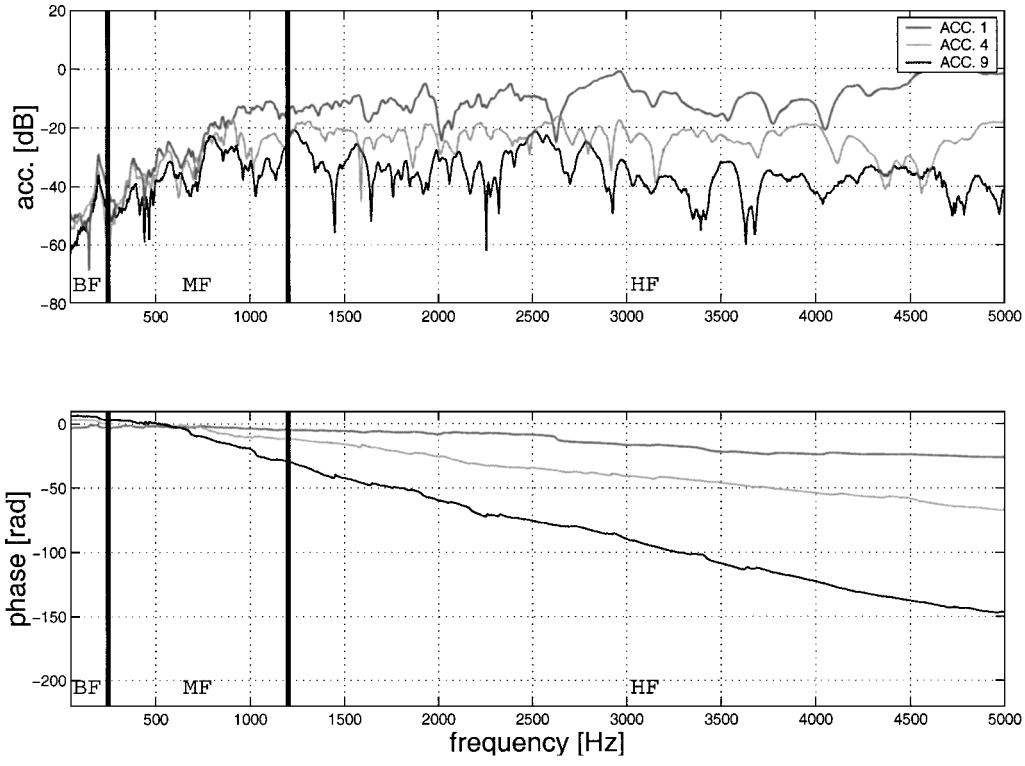

Fig. 7 Measured vertical accelerations by accelerometers 1, 4, and 9 of the first set and excitation FX3. $dB_{ref} = 20 \times \log_{10}(1\ m/s^2)$.

Influence of Uncertainties

The influence of uncertainties can be explained on the basis of a simple example taken from the books of Arnol'd[24] or Morand and Ohayon.[25] Consider an arbitrary structure occupying a bounded domain and whose eigenmodes might depend continuously on a single parameter, say τ. These eigenmodes, denoted by $\{\phi_\alpha\}_{1 \le \alpha \le N}$, and the associated eigenfrequencies, denoted by $\{\omega_\alpha\}_{1 \le \alpha \le N}$, satisfy a classical eigenvalue problem:

$$\boldsymbol{K}\phi_\alpha = \omega_\alpha^2 \boldsymbol{M}\phi_\alpha \tag{2}$$

The eigenmodes define an orthogonal transform, which diagonalizes the symmetric, positive definite matrices $\boldsymbol{M}$ and $\boldsymbol{K}$ simultaneously (whose existence is ensured by a classical result of linear algebra); we choose to normalize them with respect to the mass: $\phi_\alpha^T \boldsymbol{M} \phi_\beta = \delta_{\alpha\beta}$, where T stands for transposition. Let us now introduce a perturbation $\boldsymbol{V}(\tau)$ of the stiffness matrix such that the set of admissible displacements remains unchanged. Then the eigenvalues $\{\tilde{\omega}_\alpha\}_{1 \le \alpha \le N}$ of the perturbed structure satisfy

$$\left(\omega_\alpha^2 \delta_{\alpha\beta} + \boldsymbol{V}_{\alpha\beta}\right) q_\beta = \tilde{\omega}_\alpha^2 \delta_{\alpha\beta} q_\beta \tag{3}$$

where the $\{q_\alpha\}_{1 \le \alpha \le N}$ are the coordinates of the eigenmodes of the perturbed structure, denoted by $\{\tilde{\phi}_\alpha\}_{1 \le \alpha \le N}$, when projected on the unperturbed eigenmodes, and $V_{\alpha\beta}$ is the projection of $\boldsymbol{V}$ on ϕ_α and ϕ_β. When the perturbed eigenmodes are sought as a linear combination of two unperturbed eigenmodes associated to two successive single eigenvalues $\omega_1^2 < \omega_2^2$ (two-modes approximation), we obtain

$$\tilde{\omega}_\pm^2 = \tfrac{1}{2}\left(\lambda_1 + \lambda_2 \pm \Delta^{\frac{1}{2}}\right)$$

$$\tilde{\phi}_\pm = \Delta^{-\frac{1}{4}}\left(\pm \left|\lambda_2 - \tilde{\omega}_\pm^2\right|^{\frac{1}{2}} \phi_1 + \left|\lambda_1 - \tilde{\omega}_\pm^2\right|^{\frac{1}{2}} \phi_2 \right) \tag{4}$$

with $\lambda_\alpha = \omega_\alpha^2 + V_{\alpha\alpha}$ and $\Delta = (\lambda_1 - \lambda_2)^2 + 4V_{12}^2$. The perturbed eigenvalues are generally not repeated because the case $\Delta = 0$ leads to two equations for one unknown (τ). Two cases arise:

1) $2V_{12} \ll |\lambda_1 - \lambda_2|$: this is the so-called weak interaction. Then $\tilde{\omega}_-^2 \simeq \lambda_1$, $\tilde{\omega}_+^2 \simeq \lambda_2$, $\tilde{\phi}_- \simeq -\phi_1$, and $\tilde{\phi}_+ \simeq \phi_2$. Perturbations have introduced only a slight shift of the eigenvalues and the eigenmode directions.

2) $2V_{12} \gtrsim |\lambda_1 - \lambda_2|$: this is the so-called strong interaction. Eigenmodes are significantly altered, and the particular case $\lambda_1 = \lambda_2$ gives $\tilde{\phi}_- = (-\phi_1 + \phi_2)/\sqrt{2}$ and $\tilde{\phi}_+ = (\phi_1 + \phi_2)/\sqrt{2}$, that is, an overall rotation of 45 deg of the modes.

Note that consideration of a perturbation of the mass matrix leads to comparable results. A symmetric system with three degrees of freedom has also been considered in Ref. 26.

The strong interaction case shows that for a structure which has comparable eigenvalues a weak perturbation, or uncertainty, of the stiffness induces strong modifications to its response, at least locally. The overall space of admissible displacements is basically unchanged, but the vectors of its eigenmode basis can be significantly altered. Complex structures that exhibit a repetitive pattern of any kind, but not necessarily periodic, as for example the present experimental structure, are therefore subjected to strong interaction effects. This physical observation has important implications on the numerical strategy to be chosen: it means that it is unrealistic to compute local eigenmodes for such systems unless model uncertainties have been significantly reduced. Thus, for broadband excitations and particularly midfrequency vibrations it is generally not possible to use reduction methods based on the projection on the eigenmode basis. Furthermore, it is worth noting at this stage that the extraction of higher-order eigenmodes from a large eigenvalue problem sets important algebraic and numerical difficulties as well. However, one can remark that, although local eigenmodes might be individually strongly altered by the uncertainties, their combination should remain rather stable as indicated in the preceding remarks. The modal hybridization method proposed by Morand[18] relies on this fact to construct a reduction basis adapted to midfrequency vibrations and which is strongly dependent on the imposed excitations. The frequency window method of component mode synthesis proposed by Min et al.[27] is also reminiscent of this latter property.

Numerical Simulations of the Midfrequency Vibrations

Modeling Strategy

From the examination of the experimental results for the broadband vibrations of a complex three-dimensional structure presented in the preceding section, we have outlined several key features that numerical simulations should be able to reproduce in the midfrequency range we focus on. They orientate the modeling strategy we should adopt for the analysis of the present experimental structure.

First, analytical methods cannot be applied as a result of the evident complexity of this structure. Therefore we turn out to numerical methods. Classical linear elasticity shall be relevant for the low- to midfrequency range of interest, say $\mathcal{B} = 100$–1200 Hz, so that a variational formulation in the frequency domain discretized by the finite element method seems well adapted to our objectives. It allows the accounting for the proper boundary conditions, as well as the modeling of damping effects. For instance, a visco-elastic behavior with memory can be modelized by considering frequency-dependent stiffness and damping operators. This model is retained for the numerical simulation presented here; its relevance for the midfrequency range has already been demonstrated in Ref. 28.

The finite element mesh should incorporate a large number of degrees of freedom to cope with the typical wavelengths observed in the frequency range $\mathcal{B}$. As modal reduction cannot be directly applied in this case, for the physical and numerical reasons just outlined (considering also the fact that the stiffness matrix depends on the frequency in the general case) a direct inversion method of the whole dynamic stiffness matrix of the structure shall be implemented. To avoid the highly expensive computation of this inverse at each frequency point for the range $\mathcal{B}$, we have implemented a time-frequency algorithm,[7,8] which allows the calculation to be performed only for the central frequencies of narrow midfrequency bands whose union is the entire frequency range $\mathcal{B}$.

Time-Frequency Algorithm

A detailed presentation of the algorithm has already been made in Refs. 7–9. We briefly outline its main steps in the present section. A narrow midfrequency band B_ν is defined by its central circular frequency Ω_ν and its bandwidth $\Delta\omega_\nu$, such that

$$B_\nu = (\Omega_\nu - \Delta\omega_\nu/2,\ \Omega_\nu + \Delta\omega_\nu/2) \tag{5}$$

with $\Delta\omega_\nu \ll \Omega_\nu$ and $\mathcal{B} = \cup_\nu B_\nu$.

The weak formulation of the equation of motion of the structure in the narrow frequency band B_ν is discretized by the projection on a finite element basis, which leads to the usual following equation for all $\omega \in B_\nu$:

$$[-\omega^2 \boldsymbol{M} + i\omega \boldsymbol{D}(\omega) + \boldsymbol{K}(\omega)]\boldsymbol{U}_\nu(\omega) = \boldsymbol{F}_\nu(\omega) \tag{6}$$

Damping and stiffness matrices depend on the circular frequency because the elasticity tensor is frequency dependent for the general case of material visco-elasticity with memory. This dependence is particularly apparent in the intermediate-frequency range, whereas it is often hardly noticeable in the low-frequency range.[28] Because functions $\omega \mapsto \boldsymbol{D}(\omega)$ and $\omega \mapsto \boldsymbol{K}(\omega)$ are also continuous and usually smooth enough on the whole real line and considering that $\Delta\omega_\nu \ll \Omega_\nu$, the preceding Eq. (6) is approximated by

$$\left[-\omega^2 \boldsymbol{M} + i\omega \boldsymbol{D}(\Omega_\nu) + \boldsymbol{K}(\Omega_\nu)\right]\underline{\boldsymbol{U}}_\nu(\omega) = \boldsymbol{F}_\nu(\omega) \tag{7}$$

Equation (7) is associated to the second-order ordinary differential equation with constant coefficients:

$$\boldsymbol{M}\ddot{\underline{\boldsymbol{U}}}_\nu(t) + \boldsymbol{D}(\Omega_\nu)\dot{\underline{\boldsymbol{U}}}_\nu(t) + \boldsymbol{K}(\Omega_\nu)\underline{\boldsymbol{U}}_\nu(t) = \boldsymbol{F}_\nu(t) \tag{8}$$

Performing a change of variable $\omega = \omega' + \Omega_\nu$ in Eq. (7) with $\omega \in B_\nu$ and $\omega' \in B_0 = [-\Delta\omega_\nu/2,\ \Delta\omega_\nu/2]$, the equation obtained is solved numerically backward in time by a Newmark scheme for the long timescale $2\pi/\Delta\omega_\nu$. The approximated displacements $\underline{\boldsymbol{U}}_\nu$ in the narrowband B_ν, corresponding to the short timescale $2\pi/\Omega_\nu$, are reconstructed exactly from these numerical results by Shannon's sampling theorem. The time-frequency algorithm allows the computation of $\underline{\boldsymbol{U}}_\nu(\omega)$ for any ω in B_ν at a numerical cost theoretically comparable to the direct inversion of Eq. (6) at a single frequency in the narrowband B_ν. The final solution for the whole frequency range $\mathcal{B}$ is obtained as

$$\boldsymbol{U}(\omega) \simeq \sum_\nu \mathbf{1}_{B_\nu}(\omega)\underline{\boldsymbol{U}}_\nu(\omega) \tag{9}$$

This algorithm has been tested extensively at ONERA for simple and more complex configurations, including coupled fluid-structure interaction in structural acoustics applications, for models of slender structures up to about 30,000 degrees of freedom and 2% of nonzero terms for the stiffness matrices.

Application to the Experimental Structure

A finite element model has been developed for the experimental structure. It comprises 86,939 degrees of freedom for 16,349 nodes and 38,394 elements, including 35,166 shell elements and 3,228 beam elements. Internal acoustic cavities have not been modeled for the reasons already mentioned in the section describing the experimental setup. The numbering of equations has been optimized using the Gibbs–Poole–Stockmeyer algorithm[29] for sparse storage.

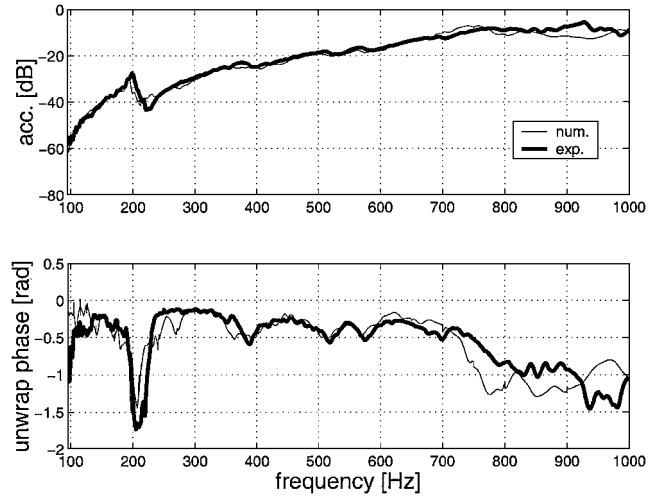

Fig. 8 Comparison of measured (——) and computed (——) auto-transfers for excitation FX3. $dB_{ref} = 20 \times \log_{10}(1\ m/s^2)$.

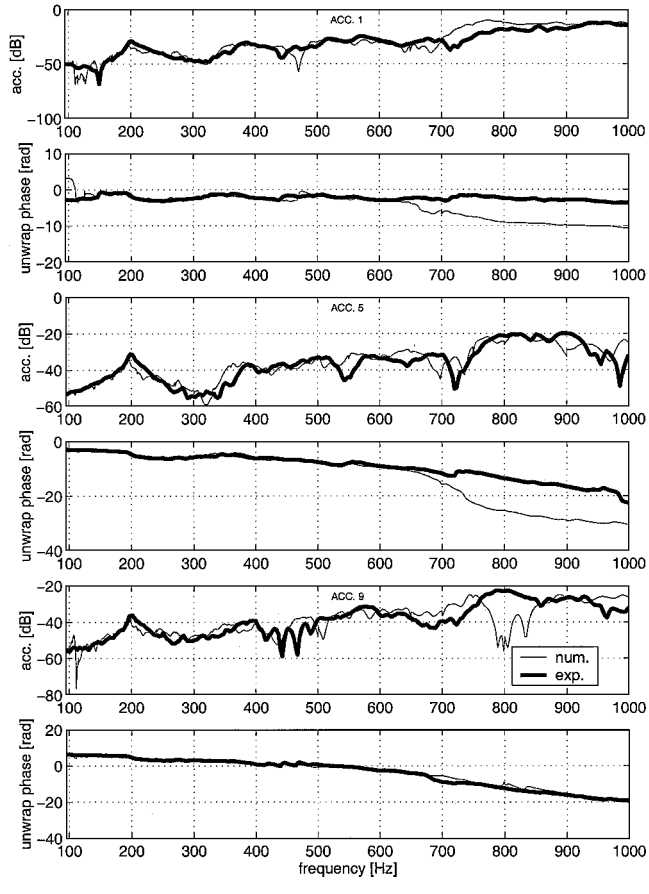

Fig. 9 Comparison of measured (——) and computed (——) cross transfers of accelerometers 1, 5, and 9 (transverse accelerations) of the first set for excitation FX3. $dB_{ref} = 20 \times \log_{10}(1\ m/s^2)$.

The density of nonzero terms in the upper triangular part of the stiffness matrix is about 0.02% for a mean half-bandwidth equal to 6%. As we want to use it for further studies in case of nonsymmetric impedance boundary conditions, no symmetry conditions were applied, and the whole structure has been discretized, although it is symmetric with respect to its longitudinal axis.

The overall frequency range of numerical analysis $\mathcal{B}_{\text{num}} = 100$–1000 Hz has been devided into 24 narrow subbands B_ν of increasing widths, the latter being fixed by the criteria $\Delta\omega_\nu/\Omega_\nu \simeq 0.1$ for $\nu = 1, 2, \ldots, 24$. Damping is taken into account throughout the analysis by a simplified model of the damping matrix, which is given the form

$$\boldsymbol{D}_\nu = \zeta_\nu \Omega_\nu \left[\boldsymbol{M} + 1\Big/\left(\Omega_\nu^2 - \Delta\omega_\nu^2/4\right)\boldsymbol{K}_\nu\right] \tag{10}$$

The average damping rate ζ_ν in the narrow frequency band B_ν is equal to 0.75% for all $\nu = 1, 2, \ldots, 24$; this value has been fixed after comparisons with the experimental results for the frequency response functions.

Calculations have been performed using the commercial code MSC/NASTRAN in which the time-frequency algorithm has been implemented in Direct Matrix Abstraction Program (DMAP) instructions. No particular care has been taken on the optimization of the program (which uses sparse matrices), but the improvement in terms of CPU time compared to a direct inversion method on a frequency-by-frequency basis is significant. The vectorized computation for one narrow frequency band and the reconstruction at 100 frequency points in that band takes 17 min of CPU time, to be compared to 2 min of CPU time for the direct inversion at a single frequency; thus the gain is a factor of about 10.

Comparisons with Experimental Observations and Lessons Pertaining to Them

We present here only the results obtained for the example of excitation FX3. Numerical results for the other excitations call for qualitatively comparable comments. Figure 8 is a plot of the frequency response function at the point where excitation FX3 is applied parallel to the x axis. Figure 9 is the plot of the frequency response functions at the locations of accelerometers 1, 4, and 9 of the first set. Finally, Fig. 10 is the plot of the estimated mechanical energies using Eq. (1) integrated over narrow frequency subbands, for both the measured and computed responses:

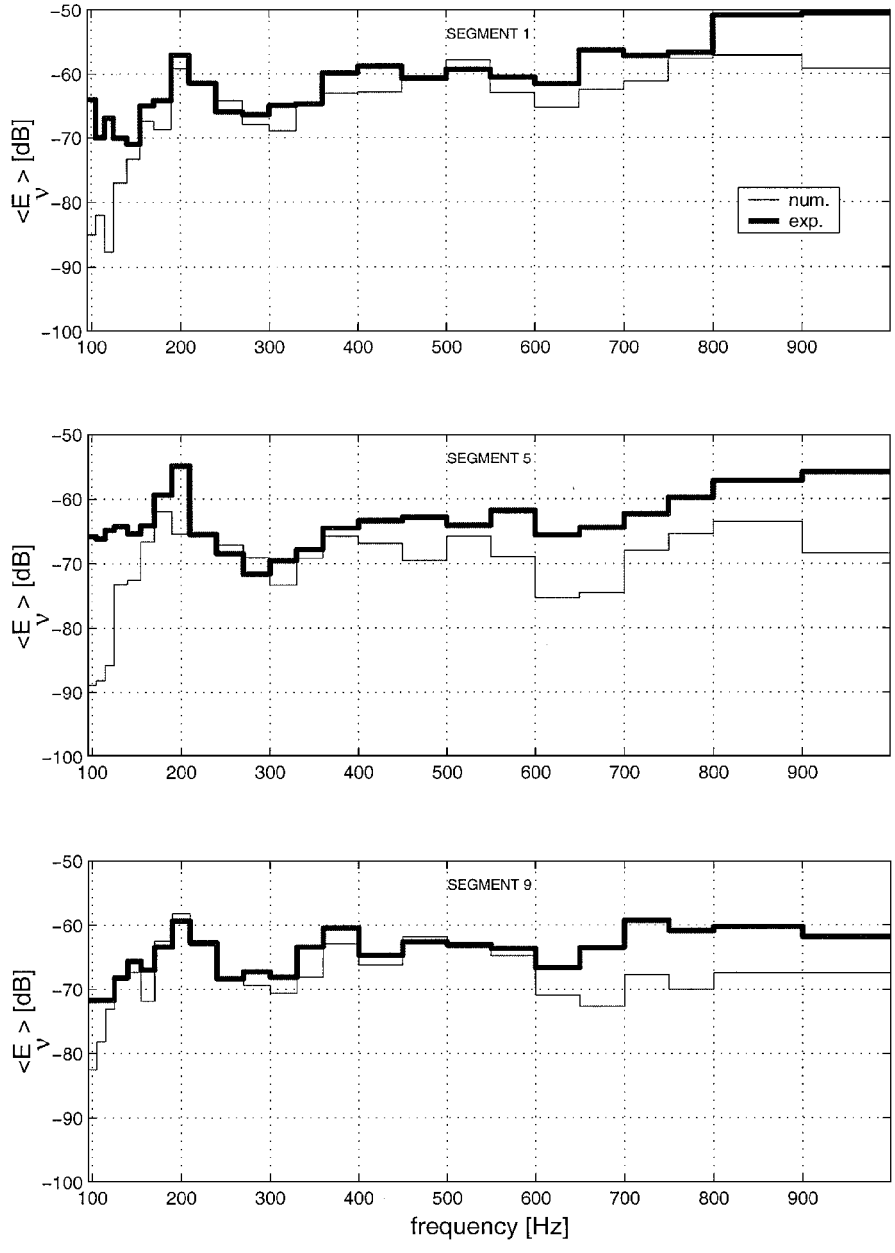

Fig. 10 Comparison of measured (——) and computed (——) mechanical energies in segments 1, 5, and 9 for excitation FX3. dB_{ref} = 10 × $\log_{10}$(1 kg · m^2/s^3).

$$\langle E_{s,v} \rangle = \frac{1}{\pi} \int_{B_v} \langle e_s(\omega) \rangle \, \mathrm{d}\omega \tag{11}$$

Numerical simulations and experimental results compare satisfactorily up to 700 Hz for the frequency response functions and up to 600 Hz for the mechanical energies. (The estimator used for these quantities is rather coarse, and anyhow it is not adapted to the low-frequency range as seen on the plots.) Clearly, the latter limitation is caused by the inadequacy of the finite element model in term of number of degrees of freedom for the higher frequencies, as further shown by the comparison of the frequency response functions for the accelerometers of sets 2 through 4 (not displayed in this communication). Indeed the typical size of the plate and beam elements is twice the average spacing between the rivets. Therefore refinement of the mesh is still possible. However, the question raised by these results is the relevance of pursuing such a strategy of refinement. The size of the elements would rapidly reach the average spacing between the rivets; thus, more sophisticated models of mechanical junctions and connections would be needed. The latter should account for both geometrical (contact, friction) and material (plasticity) local nonlinearities, for instance. To the best of our knowledge, no universal and well-established procedure has been proposed yet allowing to use them in routine applications. Furthermore this approach adds uncertainty to the problem in the sense that a refined mesh would require a great deal of refined estimation of the (increasingly numerous) parameters input in the model and their levels of confidence. Nevertheless, one can conjecture that a routine finite element analysis is always able to predict the structural dynamic behavior in some lower part of the midfrequency range, provided that a direct inversion of the dynamic stiffness matrix is performed.

But this case study, considered as a characteristic one of industrial applications (for instance a military aircraft fuselage), underlines the difficulties put by the development of numerical tools for the prediction of vibrations in the upper part of the midfrequency range as just defined, as well as its transition with the high-frequency range. Indeed Figs. 6 and 7 show that a truly complex structure has a completely different dynamic behavior whether it is observed in the low-frequency range or in the high-frequency range. Global standing waves, the global normal modes, dominate in the former, whereas a typical transport or diffusive pattern is observed in the latter. It is very much unlikely that the same mathematical model and numerical method can describe both behaviors. For instance, steady-state or transient SEA equations have a fundamentally different mathematical structure as compared to the classical structural dynamics equation (6). In the intermediate-frequency range there is a transition between two dynamic behavior patterns; therefore, there should be a transition of numerical models as well. We can consider several different strategies, having all their own limitations. Multiscale approaches, for the present case, raise questions whether it is possible to define different spatial scales for such a heterogeneous, bounded structure. A possible way to overcome these difficulties would be to use nonparametric models,[30] at least to model local uncertainties corresponding to the mechanical junctions in conjunction with substructuring techniques in the finite element method. The same questions arise with the implementation of SEA, hybrid SEA, or power flow methods[13–15] being foreseen, whereas their application to the present case for the high-frequency range seems feasible at first glance; their extension to the upper part of the midfrequency range identified here raises challenging questions. On the other hand, asymptotic ray methods[16] could not properly handle the boundary conditions and the topology of such a structure and thus would require adapted treatments for these aspects. Further research is clearly needed in this direction, and one of the aims of this study is to show that the proposed numerical methods should be applicable to arbitrary, complex configurations and topologies that exhibit the most characteristic features and difficulties raised by midfrequency vibration predictions.

As regards experimental aspects, one can make the following concluding remark for the time being. An interesting aspect of the numerical reduction bases proposed in Refs. 19–21 is that they can be constructed from measured responses on one hand and that they fully integrate the fact that these responses are highly dependent on the shape of the excitations, at least in the midfrequency range, on the other hand. Their intensive use requires the development of appropriate acquisition procedures in order to construct transfer response functions of high dimensions. Automated laser vibrometers can partially fulfill such needs and bring further insights into the midfrequency range of vibrations.

Conclusions

This paper has presented a tentative experimental validation of some numerical methods currently implemented for the prediction of vibrations of complex structures in the midfrequency range. The experimental data have been used to give further evidences of the typical behavior of a truly complex structure in the intermediate-frequency range and to elaborate a modeling strategy adapted to these frequencies. Comparisons between measurements and numerical simulations show a good agreement for the lower part of the frequency range of interest, which validates a posteriori the strategy chosen, but the model developed fails to properly predict the structural response characteristics in its upper part. Although the origin of this inefficiency can be clearly identified, it raises questions whether such predictions are realizable with the actual numerical methods in cases of realistic complex structures. This study has underlined the need to enhance the numerical methods used for midfrequency vibration predictions, which should be able to account for an arbitrary complex topology, typically assemblies of beams, plates, and shells rather than those simple structural elements.

Acknowledgments

Financial support from the Direction Générale de l'Armement/Service des Programmes Aéronautiques is gratefully acknowledged. All experiments were carried out by Pascal Baroin, François Bisciglia, and Michel Menelle.

References

[1]Friswell, M. J., and Mottershead, J. E., *Finite Element Model Updating in Structural Dynamics*, Kluwer, Dordrecht, The Netherlands, 1995.

[2]Ihlenburg, F., and Babuška, I., "Finite Element Solution of the Helmholtz Equation with High Wave Number. Part 2: the h-p Version of the FEM," *SIAM Journal on Numerical Analysis*, Vol. 34, No. 1, 1997, pp. 315–358.

[3]Dey, S., Shirron, J. J., and Couchman, L. S., "Mid-Frequency Structural Acoustic and Vibration Analysis in Arbitrary, Curved Three-Dimensional Domains," *Computers and Structures*, Vol. 79, No. 6, 2001, pp. 617–629.

[4]Hughes, T. J. R., "Multiscale Phenomena: Green's Functions, the Dirichlet-to-Neumann Formulation, Subgrid Scale Models, Bubbles and the Origins of Stabilized Methods," *Computer Methods in Applied Mechanics and Engineering*, Vol. 127, No. 3–4, 1995, pp. 387–401.

[5]Ben Dhia, H., "Numerical Modeling of Multiscale Mechanical Problems: the Arlequin Method," *Comptes Rendus de l'Académie des Sciences*, Vol. 326, Série IIb, No. 12, 1998, pp. 899–904.

[6]Strouboulis, T., Babuška, I., and Copps, K., "The Design and Analysis of the Generalized Finite Element Method," *Computer Methods in Applied Mechanics and Engineering*, Vol. 181, No. 1–3, 2000, pp. 43–69.

[7]Soize, C., "Medium Frequency Linear Vibrations of Anisotropic Elastic Structures," *La Recherche Aérospatiale* (English ed.), Vol. 5, Sept.–Oct. 1982, pp. 65–87.

[8]Soize, C., Hutin, P.-M., Desanti, A., David, J.-M., and Chabas, F., "Linear Dynamic Analysis of Mechanical Systems in the Medium Frequency Range," *Computers and Structures*, Vol. 23, No. 5, 1986, pp. 605–637.

[9]Liu, W. K., Zhang, Y., and Ramirez, M. R., "Multiple Scale Finite Element Methods," *International Journal for Numerical Methods in Engineering*, Vol. 32, No. 5, 1991, pp. 969–990.

[10]Burie, J. B., and Marion, M., "Multilevel Methods in Space and Time for the Navier–Stokes Equations," *SIAM Journal on Numerical Analysis*, Vol. 34, No. 4, 1997, pp. 1574–1599.

[11]Greenstadt, J., "Solution of Wave Propagation Problems by the Cell Discretization Method," *Computer Methods in Applied Mechanics and Engineering*, Vol. 174, No. 1–2, 1999, pp. 1–21.

[12]Sestieri, A., Del Vescovo, D., and Lucibello, P., "Structural-Acoustic Coupling in Complex Shaped Cavities," *Journal of Sound and Vibration*, Vol. 96, No. 2, 1984, pp. 219–233.

[13]Langley, R. S., and Bremner, P., "A Hybrid Method for the Vibration Analysis of Complex Structural-Acoustic Systems," *Journal of the Acoustical Society of America*, Vol. 105, No. 3, 1999, pp. 1657–1671.

[14]Yan, H., Parrett, A., and Nack, W., "Statistical Energy Analysis by Finite Elements for Middle Frequency Vibration," *Finite Elements in Analysis and Design*, Vol. 35, No. 4, 2000, pp. 297–304.

[15] Vlahopoulos, N., and Zhao, X., "Basic Development of Hybrid Finite Element Method for Midfrequency Structural Vibrations," *AIAA Journal*, Vol. 37, No. 11, 1999, pp. 1495–1505.

[16] Ladevèze, P., "A New Computational Approach for Structure Vibrations in the Medium Frequency Range," *Comptes Rendus de l'Académie des Sciences*, Vol. 322, Série IIb, No. 12, 1996, pp. 849–856.

[17] Guyader, J.-L., "Modal Sampling Method for the Vibration Study of Systems of High Modal Density," *Journal of the Acoustical Society of America*, Vol. 88, No. 5, 1990, pp. 2269–2276.

[18] Morand, H. J.-P., "A Modal Hybridization Method for the Reduction of Dynamic Models in the Medium Frequency Range," *European Conference on New Advances in Computational Structural Mechanics, Giens, 2–5 April 1991*, edited by P. Ladevèze and O. C. Zienkiewicz, Vol. 32, Studies in Applied Mechanics, Elsevier Science, Amsterdam, 1992, pp. 347–364.

[19] Soize, C., "Reduced Models in the Medium Frequency Range for General Dissipative Structural-Dynamics Systems," *European Journal of Mechanics A/Solids*, Vol. 17, No. 4, 1998, pp. 657–685.

[20] Kim, T., "Frequency-Domain Karhunen–Loève Method and Its Application to Linear Dynamic Systems," *AIAA Journal*, Vol. 36, No. 11, 1998, pp. 2117–2123.

[21] Ma, X., Vakakis, A. F., and Bergman, L. A., "Karhunen-Loève Modes of a Truss: Transient Response Reconstruction and Experimental Verification," *AIAA Journal*, Vol. 39, No. 4, 2001, pp. 687–696.

[22] Bisciglia, F., Menelle, M., and Baroin, P., "Validation of Numerical Methods for the Taking into Account of Structural Complexity. Experimental Study," ONERA, Tech. Rept. RT 2/03128 DDSS, Châtillon, France, May 2001.

[23] Gibert, Ph., "Low and Medium Frequencies in Highly Heterogeneous Structures," *Comptes Rendus de l'Académie des Sciences*, Vol. 295, Série II, 1982, pp. 951–954.

[24] Arnol'd, V., *Mathematical Methods of Classical Mechanics*, Springer-Verlag, New York, 1978, Appendix 10.

[25] Morand, H. J.-P., and Ohayon, R., *Fluid Structure Interaction*, Wiley, New York, 1995, pp. 14–17.

[26] Balmès, E., "High Modal Density, Curve Veering, Localization: a Different Perspective on the Structural Response," *Journal of Sound and Vibration*, Vol. 161, No. 2, 1993, pp. 358–363.

[27] Min, K.-W., Igusa, T., and Achenbach, J. D., "Frequency Window Method for Strongly Coupled and Multiply Connected Structural Systems: Multiple-Mode Windows," *Journal of Applied Mechanics*, Vol. 59, No. 2, Pt. 2, 1992, pp. S244–S252.

[28] Ohayon, R., and Soize, C., *Structural Acoustics and Vibration*, Academic Press, London, 1998, pp. 61–127.

[29] Gibbs, N. E., Poole, W. G., and Stockmeyer, P. K., "An Algorithm for Reducing the Bandwidth and Profile of a Sparse Matrix," *SIAM Journal on Numerical Analysis*, Vol. 13, No. 2, 1976, pp. 236–250.

[30] Soize, C., "A Nonparametric Model of Random Uncertainties for Reduced Matrix Models in Structural Dynamics," *Probabilistic Engineering Mechanics*, Vol. 15, No. 3, 2000, pp. 277–294.

A. Berman
Associate Editor